Title
Invar Metal Matrix Composites

Author
Moz, Melissa Kathryn

Publication Date
2018

Peer reviewed|Thesis/dissertation

UNIVERSITY OF CALIFORNIA

Los Angeles

Invar Metal Matrix Composites

A thesis submitted in partial satisfaction

of the requirements for the degree Master of Science

in Materials Engineering

by

Melissa Kathryn Moz

2018

ABSTRACT OF THE THESIS

Invar Metal Matrix Composites

by

Melissa Kathryn Moz

Master of Science in Materials Engineering

University of California, Los Angeles, 2018

Professor Bruce Dunn, Chair

Invar metal matrix composites, incorporating amorphous silica ranging from 0-50vol%, were produced with the intention of processing the composites using additive manufacturing. These composites were aimed to have a lower density and CTE than that of pure Invar. Densities ranging from 7.44 g/cm^3 (92% of theoretical) to 4.79 g/cm^3 (93% of theoretical) were attained for pure Invar and the 50/50 composite respectively when sintered at 1250^{o}C for 5 hours. These high temperatures were necessary to sinter the silica-rich regions of the composite however at temperatures exceeding 1200^{o}C, the phase separation of iron silicate was observed on the surface of 90/10 vol% samples. X-ray diffraction also found the amorphous silica would devitrify to cristobalite and tridymite during sintering. These crystalline forms of silica have a larger CTE than Invar, which resulted in a CTE increase with the addition of silica in the composites.

The thesis of Melissa Kathryn Moz is approved.

Yu Huang

Ximin He

Bruce S. Dunn, Committee Chair

University of California, Los Angeles

2018

Table of Contents

Introduction 1

Motivation 1

Objective 2

Experimental 3

Results

- X-ray Diffraction 7
- Density 13
- Microstructure Characterization 17
- Energy-Dispersive X-ray Spectroscopy 19
- Electrical Resistivity 23
- Coefficient of Thermal Expansion 24

Conclusion 28

References 30

List of Figures and Tables

Figure 1: Lowered CTE at 36wt% Ni Composition in Invar 2

Figure 2: Method of Incorporating Binder into Ball Milled Powders 5

Table 1: List of Samples Prepared, Corresponding Densities and Heat Treatment 5

Figure 3: XRD of Oxidized, Unpolished Surface of Pure Invar Sample Sintered at 1150°C for 1 hour 8

Figure 4: XRD of Samples Retaining γ-FeNi phase: Unsintered Ball Milled Invar Powder (Blue), Pure Invar Sample Sintered at 1150°C for 1 hour (Green), 75/25 Invar/Silica vol% Sample Sintered at 1150°C for 1 hour (Purple) 9

Figure 5: XRD of 50/50 Invar/Silica vol% Composite Sintered at 1150°C for 1 hour 10

Figure 6: (a) Silica Phase Diagram (b) Region of Tridymite Formation 11

Table 2: Phase Transformation of Silica 11

Figure 7: Image of Phase Separation on the Unpolished Surface of 90/10 Sample Sintered at 1250°C for 5 hours 12

Figure 8: XRD of Phase Separation on Surface of 90/10 Sample Sintered at 1250°C for 5 hours 13

Figure 9: Experimental Density vs. Silica Composition for Samples using Different Binders 14

Table 3: Average Pressed Density per Sample Composition 15

Table 4: Density Results for Sintering Parameters of Each Sample Set 15

Figure 10: Experimental Density vs. Silica Composition 16

Figure 11: SEM Images for PVDF/NMP Binder, 1150^{o}C-1hr 17

Figure 12: 50/50 vol% Invar/Silica Samples 1150^{o}C-3hrs (left), 1250^{o}C-5hrs (right) 18

Figure 13: EDX of Compositions of 2 Regions on the Surface of 90/10 vol% Invar/Silica Sintered at 1250^{o}C for 5 hours (a) an image of the region scanned (b) Composition of Point 1 Showing No Presence of Ni (c) Composition of Point 2 Showing Ni in the Bulk of the Sample 19

Figure 14: EDX for 50/50 Composition Sintered at 1150^{o}C for 1 hour 21

Figure 15: EDX for 50/50 Composition Sintered at 1250^{o}C for 5 hours 22

Table 5: Electrical Resistivity based on Silica Composition 23

Figure 16: Displacement Curves for 1150^{o}C-3hrs Samples at Different Invar/Silica vol% Ratios 24

Figure 17: Average CTE for Across Different Temperature Ranges for 25

Samples Sintered at 1150^{o}C for 3 hours

Table 6: Average CTE Values Across Different Temperature Ranges for 25

Samples Sintered at 1150^{o}C for 3 hours

Figure 18: Displacement Curves for 1250^{o}C-5hrs Samples at Different 26

Invar/Silica vol% Ratios

Figure 19: Average CTE for Across Different Temperature Ranges for 27

Samples Sintered at 1250^{o}C for 5 hours

Table 7: Average CTE Values Across Different Temperature Ranges for 27

Samples Sintered at 1250^{o}C for 5 hours

Acknowledgements

I would first like to thank my thesis advisor Dr. Dunn at UCLA for giving me the opportunity to conduct research in his lab. The knowledge I have gained over my time here is invaluable and I am so grateful for the experience. He provided me with so much guidance and support along the way.

I would also like to thank Dr. Lan who helped me set up my research plan and get familiarized in lab. She also provided me with advice that I found extremely helpful and will take with me even after I leave UCLA.

I am also grateful to JPL for funding and supporting this research. Thank you to Dr. McEnerney and Dr. Bux for their guidance during the project.

A special mention to Danielle Butts, Grace Whang, and Matt Lai for their help with the characterization of my samples. Also, to everyone in Dunn Lab, thank you for all your assistance; it was great sharing the lab with all of you.

Introduction

Additive manufacturing has been gaining popularity due to its ability to increase production speeds, produce complex parts, and reduce material waste. This method of manufacturing has begun to replace CNC (computer numeric controlled) machining where material is cut away until it meets the dimensions specified in a computer program. Alternatively, powder bed additive manufacturing allows a part to be formed in a layer-by-layer process where a laser or electron beam moves over the powder bed according to a CAD (computer-aided design) program. This either melts or sinters the powders to form a solid in the specified design, then the powder bed is lowered incrementally, and the next layer is formed on top of the previous. [1-2]

The aerospace industry has been taking steps towards using more additive manufacturing parts as opposed to traditional CNC parts. Additive manufacturing can allow for more optimized, complex designs as well as the combination of multiple parts. The reduction of the number of parts needed to be welded/fastened, leads to better overall performance. Another key benefit to the use of additive manufacturing techniques, is the ability to design more complex parts that utilize less mass. Mass reduction in the aerospace industry can lead to significant cost reduction in aerospace flight applications. The transition to additive manufacturing has already showed much promise with several aerospace materials such as steels, nickel alloys, aluminum alloys, and titanium alloys being found to be compatible with these techniques. [3]

Motivation

Invar was discovered by Charles Edouard Guillaume who received a Nobel Prize in Physics for demonstrating this unique alloy had a low CTE at a specific composition. [4] This advancement has led to greater improvements in scientific measurements and instrumentation. Many optical

imaging systems on spacecraft require materials that have high dimensional stability and can operate under tight tolerances. Invar (Fe-36wt%Ni) has been selected as a material to be used for such precision instruments. [5] The material's *invar*iability, particularly its low coefficient of thermal expansion (CTE as low as 1.2 x 10^{-6} /^{o}C), is what makes it of interest for these applications. Invar's unique properties have led to its extensive research and an investigation of viable processing routes. One of these methods being additive manufacturing, where Invar has been successfully 3D printed using laser melting deposition, metal injection molding, and selective laser melting. [6-9]

Figure 1: Lowered CTE at 36wt% Ni Composition in Invar [10]

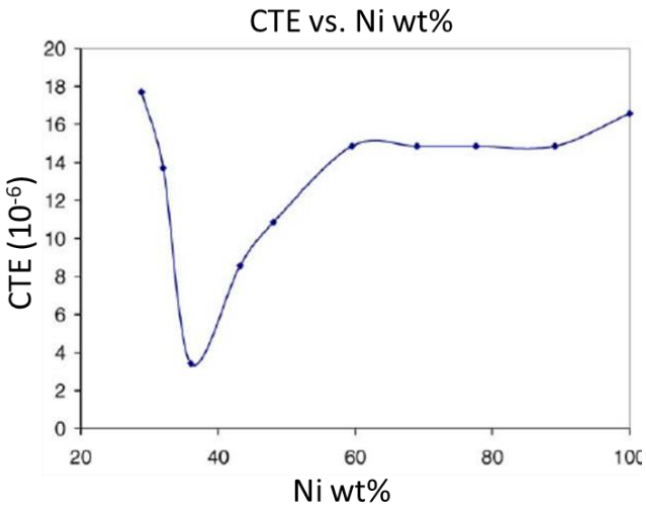

Objective

This research focused on the ability to improve upon the desirable properties of Invar while keeping the method of additive manufacturing in mind. Two properties of concern for Invar's applications in the aerospace industry are density and CTE. One route by which to modify these properties is by creating a metal-matrix composite. The method of creating metal-matrix composites to tailor specific properties has proved successful in the past by combining different

metals and ceramics. [11-15] For the aerospace applications of Invar, it would be beneficial to control the CTE of the material in order to reduce the CTE mismatch it may have with different materials. It is also desirable to be able to lower the density of Invar (8.05 g/cm^3) as a means of reducing aerospace flight cost. Amorphous silica was selected as the material to be incorporated in the composite due to its low density (2.2 g/cm^3) and CTE (0.55 x10^{-6}).

With these goals in mind, varying amounts of silica were mixed with Invar and sintered to attain dense metal matrix composites. The compositions ranged from pure Invar to 50/50 vol% Invar/silica, where a possible target would be to reach a density comparable to that of Ti (4.5g/cm^3). The CTE of the composites were also measured in the hope that the composites would have a reduced CTE compared to that of pure Invar. The composites were also characterized to better understand the microstructure and identify the formation of any new phases. The use of powder metallurgy techniques will give an indication of the capability of 3D printing and some of the parameters necessary.

Experimental

To lower the density and possibly CTE of the material, Invar and silica powder were combined at different volume ratios. The Invar iron-nickel powder (Thermo Fisher Scientific) had a particle size of ~44um in diameter and the silica amorphous nanopowder (Thermo Fisher Scientific) was ~80nm in diameter as received. Different volume ratios of Invar and silica were combined, and the powders were ball milled overnight to ensure thorough mixing. The Invar/silica vol% ratios mixed were: 100/0, 90/10, 75/25, 60/40, and 50/50. The different compositions allowed for a better understanding of the tailorability of properties such as density, CTE, and electrical conductivity.

Equation 1: Rule of Mixtures

$$X_{Composite} = X_{Invar} v_{Invar} + X_{Silica} v_{Silica} \quad [1]$$

The Rule of Mixtures as seen in Equation 1 was used when calculating the expected values for density and CTE of the composites where v is the volume fraction and X is the property of interest. These expected values were then set as the target density and CTE to reach after sintering the samples.

In some cases, polymer binders were incorporated with a solvent to help with pellet pressing. The samples with higher ratios of silica, the 60/40 and 50/50 ratios, had some difficulty being formed into a pellet without cracking. The cracks would usually form horizontally through the pellet and lead to delamination in the sintering step. Two different binders: CMC (carboxymethyl cellulose) in H_2O and PVDF (polyvinylidene difluoride) in NMP were tried to help with the forming of the pellets. These polymer binders were incorporated at very low amounts (~1wt%) and were able to reduce cracking in the samples. The use of polymer binder for formability resembles some additive manufacturing techniques, such as extrusion 3D printing. The binder and solvent were added to the ball milled powder and vortexed into a slurry. This ensured a thorough dispersion of the polymer into the powder. The solvent was then removed by placing in a drying oven (65^{o}C) overnight or on a hot plate (100^{o}C) for a few hours. Once the powder was dry, a mortar and pestle were used to break it up into a fine powder.

Figure 2: Method of Incorporating Binder into Ball Milled Powders

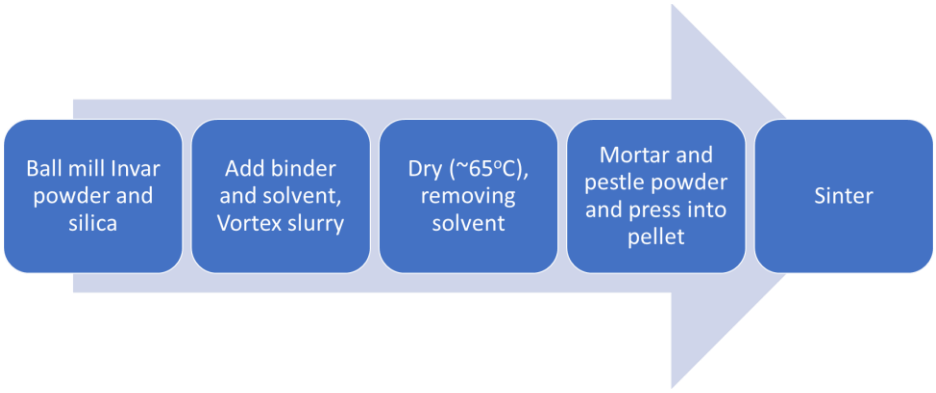

The different ratios of powders, either with or without binder, were then pressed (~10,000 lbs.) using a pellet press and die (13mm dia.). The thicknesses of the samples were aimed to be approximately 2mm for all the samples. After the pressing of samples, the diameters and thicknesses of the pellets were measured with a micrometer. The masses of the samples were also weighed to calculate the density of the pellets before sintering. Pure Invar samples would keep the diameter dimensions of the die, 13mm, when pressed. However, the samples containing larger silica ratios showed an expansion in diameter, with the 50/50 samples being ~13.22mm after pressing. The removal of the sample from the die at this stage could have been the source of the formation of cracks for the 60/40 and 50/50 samples. After the samples were pressed and measured, the pellets were then ready to be sintered. Table 1 below shows a list of the samples prepared, their densities prior to sintering, and their heat treatment.

Table 1: List of Samples Prepared, Corresponding Densities and Heat Treatment

Sample Set	Binder	Invar/Silica vol% Ratio	Sample Mass (g)	Calculated Density (g/cm^3)	Heat Treatment
1	CMC/H_2O	100/0	1.51	6.19	500°C for 1 hour 1200°C for 1 hour Ramp Rate: 5°C/min
		90/10	1.57	5.53	
		75/25	0.96	4.60	

		50/50	0.75	3.28	
2	PVDF/NMP	100/0	1.92	5.87	500°C for 1 hour 1150°C for 1 hour Ramp Rate: 3°C/min
		90/10	1.98	5.67	
		75/25	1.70	4.75	
		50/50	1.40	3.36	
3	CMC/H_2O	100/0	1.90	5.87	500°C for 1 hour 1150°C for 1 hour Ramp Rate: 3°C/min
		90/10	1.86	5.44	
		75/25	1.59	4.55	
		50/50	1.05	3.06	
4	none	100/0	2.01	6.20	1250°C for 1 hour Ramp Rate: 5°C/min up to 700°C, then 4°C/min
		90/10	1.70	5.79	
		75/25	1.47	4.89	
		50/50	1.14	3.12	
5	none	100/0	1.98	6.13	1275°C for 1 hour Ramp Rate: 5°C/min up to 700°C, then 4°C/min
		90/10	1.78	5.77	
		75/25	1.62	4.83	
		60/40	0.99	3.47	
		50/50	0.99	3.27	
6	none	100/0	1.99	6.26	1250°C for 5 hours Ramp Rate: 5°C/min up to 700°C, then 4°C/min
		90/10	1.70	5.86	
		75/25	1.41	4.63	
		60/40	0.98	2.42	
		50/50	0.79	2.16	
7	none	100/0	1.99	6.23	1100°C for 2 hours Ramp Rate: 5°C/min
		90/10	1.81	5.60	
		75/25	1.54	4.71	
		50/50	0.76	3.13	
8	none	100/0	2.00	6.17	1150°C for 3 hours Ramp Rate: 5°C/min up to 700°C, then 4°C/min
		90/10	1.77	5.71	
		75/25	1.62	4.52	
		60/40	1.01	3.62	
		50/50	0.73	3.31	

Different sintering parameters were investigated in an attempt to obtain densities closest to the theoretical full density calculated from the Rule of Mixtures. Samples were sintered in a tube furnace in flowing inert atmosphere (argon) in order to avoid the complete oxidation of the sample when heating. Prior to heating, the tube furnace would be sealed with the samples inside and left to purge for approximately an hour. The samples containing binder were heated to 500°C and held

for an hour to remove binder before heating to the sintering temperature. A variety of sintering conditions were tested: 1100^{o}C for 2hrs, 1200^{o}C for 1hr, 1150^{o}C for 1hr, 1150^{o}C for 3hr, 1250^{o}C for 1hr, 1275^{o}C for 1hr, and 1250^{o}C for 5hrs.

The samples removed from the tube furnace typically had a thin layer of oxidation which was identified through the use of X-ray Diffraction (XRD). The oxide layer was removed by polishing and then densities were measured using Archimedes method. This density was then compared to the theoretical full density to find the percent theoretical density of each of the composites. After density measurements, the samples were characterized using a variety of techniques.

Results

X-ray Diffraction

When the Invar samples were removed from the tube furnace, there appeared to be a layer of oxidation on the samples. This was confirmed by scanning the surface of the sample were the XRD results can be seen in Figure 3 below. The layer of oxidation is mainly comprised of magnetite Fe_3O_4 as indicated by the green markers. This thin layer was polished off in order to reduce the noise in the scan as well as better understand the phases present in the bulk of the sample.

Figure 3: XRD of Oxidized, Unpolished Surface of Pure Invar Sample Sintered at 1150°C for 1 hour

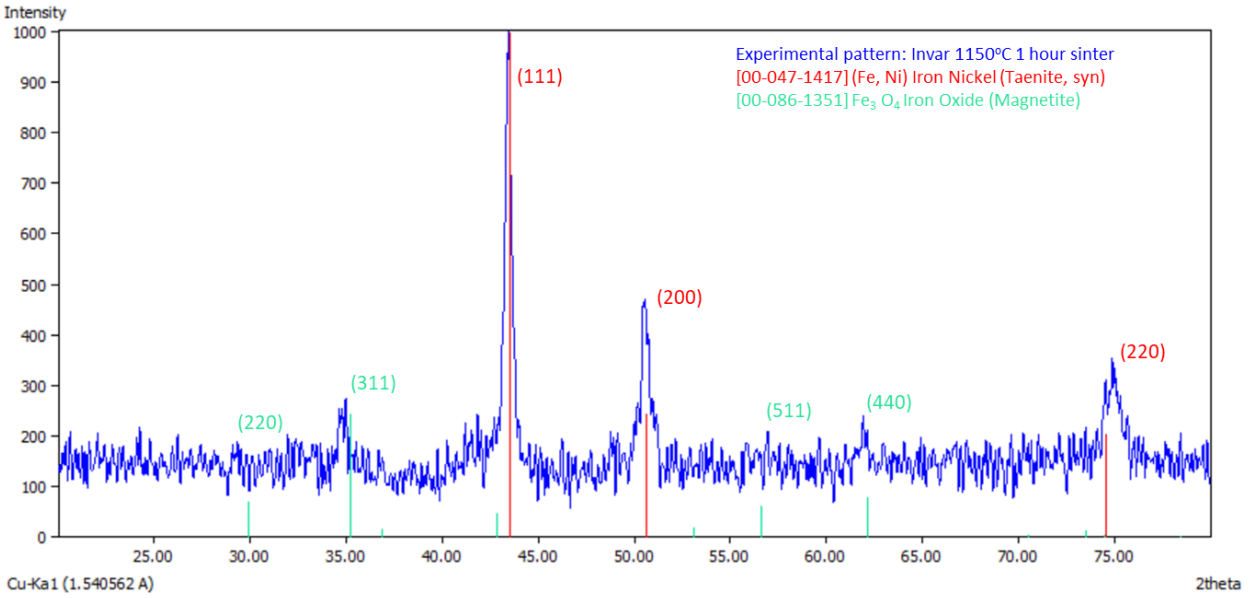

X-ray diffraction was used to identify the phases present in the sintered samples. First the ball milled, unsintered Invar powder was scanned to verify the γ-FeNi phase which is indicated by the red markers in Figure 4 below. The pure invar and 75/25 samples after showed similar peaks after sintering, indicating the γ-FeNi phase was retained. There also appears to be no evidence of oxide peaks in the samples. This suggests that once the surface oxide is polished away, there is minimal oxidation in the bulk of the sample. There is also no silica peaks present, either amorphous or crystalline, for the 75/25 sintered sample. This is most likely due to the low silica weight percent and noise in the scan.

Figure 4: XRD of Samples Retaining γ-FeNi phase: Unsintered Ball Milled Invar Powder (Blue), Pure Invar Sample Sintered at 1150°C for 1 hour (Green), 75/25 Invar/Silica vol% Sample Sintered at 1150°C for 1 hour (Purple)

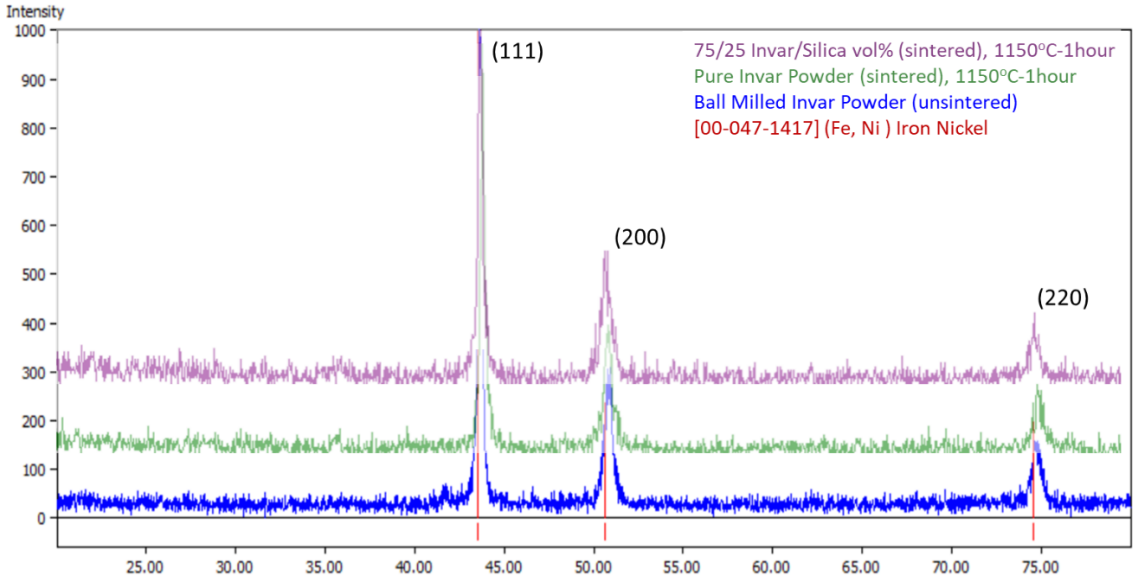

An XRD scan of the 50/50 sample after sintering, gives more information about the silica in the composite. As seen in Figure 5 below, the γ-FeNi phase peaks are still present but now with subtle peaks in the 20-25° range for 2θ. These peaks indicate the amorphous silica is most likely crystallizing at high temperatures, since a large broad peak would be expected in in this range for amorphous materials. Both tridymite and cristobalite have similar peaks in this range, so more information was needed to index the peaks.

Figure 5: XRD of 50/50 Invar/Silica vol% Composite Sintered at 1150ºC for 1 hour

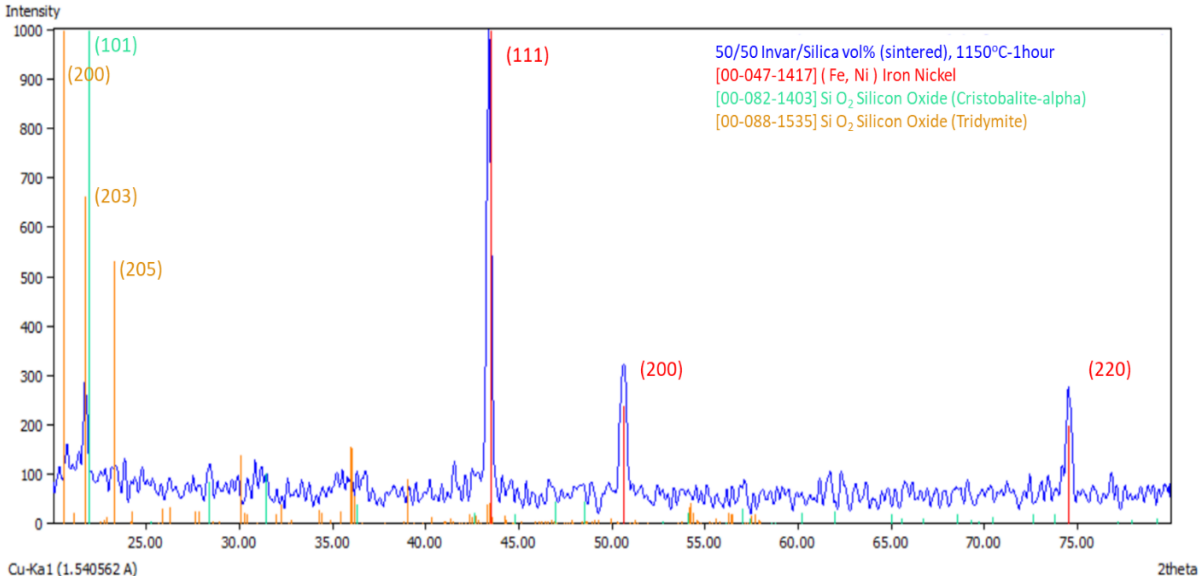

Referring to the phase diagram in Figure 6, tridymite is the stable phase for the temperature range and pressure (~0.0001 GPa) the samples were sintered. However, it has been found that cristobalite will be the first phase to form prior to any other phases during the devitrification of silica.[16] Table 2 below provides information on the phase transformation for silica, where a metastable cristobalite phase can form at 1100ºC. It should be noted that the starting temperature for devitrification is also dependent on the amount of impurities present. The samples were heated to temperatures exceeding that necessary for the silica to begin to devitrify.

Figure 6: (a) Silica Phase Diagram [17] (b) Region of Tridymite Formation

a)

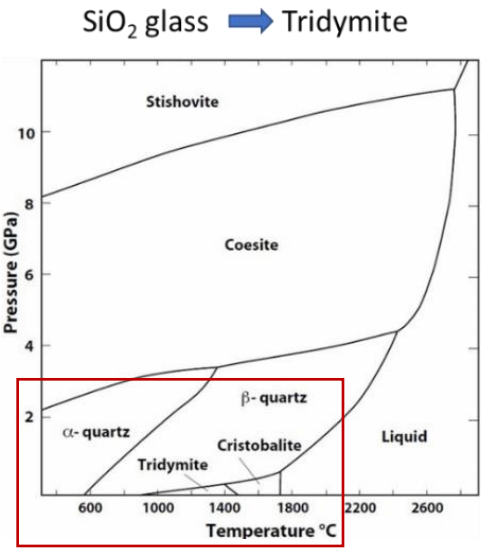

b)

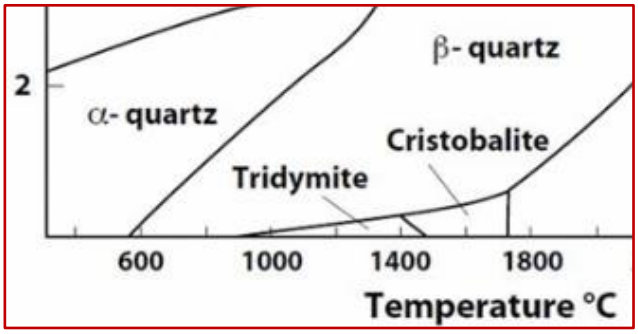

Table 2: Phase Transformation of Silica [16]

Temperature Range(s)	Transformation
Below 867°C	No transformation, stable.
867°C - 1450°C	Devitrifies above 1100°C into cristobalite
Above 1450°C	Stable cristobalite

The XRD peaks in the 50/50 vol% Invar/Silica sample in Figure 5, provide more information as to whether the metastable cristobalite or stable tridymite phase are present in the samples. The cristobalite peaks are shown in green and tridymite peaks are shown in orange. Based on the intensity of the peaks, cristobalite appears to be present but there are also lower intensity peaks suggesting the formation of tridymite. These crystalline forms of silica are not desired as they have different density and CTE than that of amorphous silica. These different phases could therefore change the properties of the sintered composites.

One main concern when sintering these composites, is the undesired formation of Fe silicate phases. Based on the XRD results of the polished samples, there appear to be no such phases present. However, there appeared to be phase separation on the surface of the 90/10 samples sintered at 1250 ^{o}C which was visually distinct from the rest of the sintered Invar sample. An image of such phase separation is shown in the unpolished sample below in Figure 7. At first, it was believed to be due to contamination or poor mixing of the silica and Invar powders. However, the same results occurred even after ball milling a new set of powder in a new container.

Figure 7: Image of Phase Separation on the Unpolished Surface of 90/10 Sample Sintered at 1250^{o}C for 5 hours

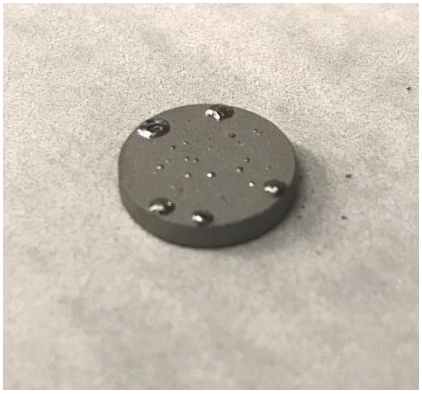

A normal incidence XRD scan of the surface of the sample is shown in Figure 8 below. Some of the peaks are due to the iron oxide layer on the unpolished sample. However, there still are other unidentified peaks. It was found that they resemble that of iron silicate which is indicated by the orange colored markers. Due to the low intensity of the peaks and noise in the scan, the identification of iron silicate in the XRD scan was not definitive. This phase separation on the surface of the sample was therefore investigated further using other methods.

Figure 8: XRD of Phase Separation on Surface of 90/10 Sample Sintered at 1250°C for 5 hours

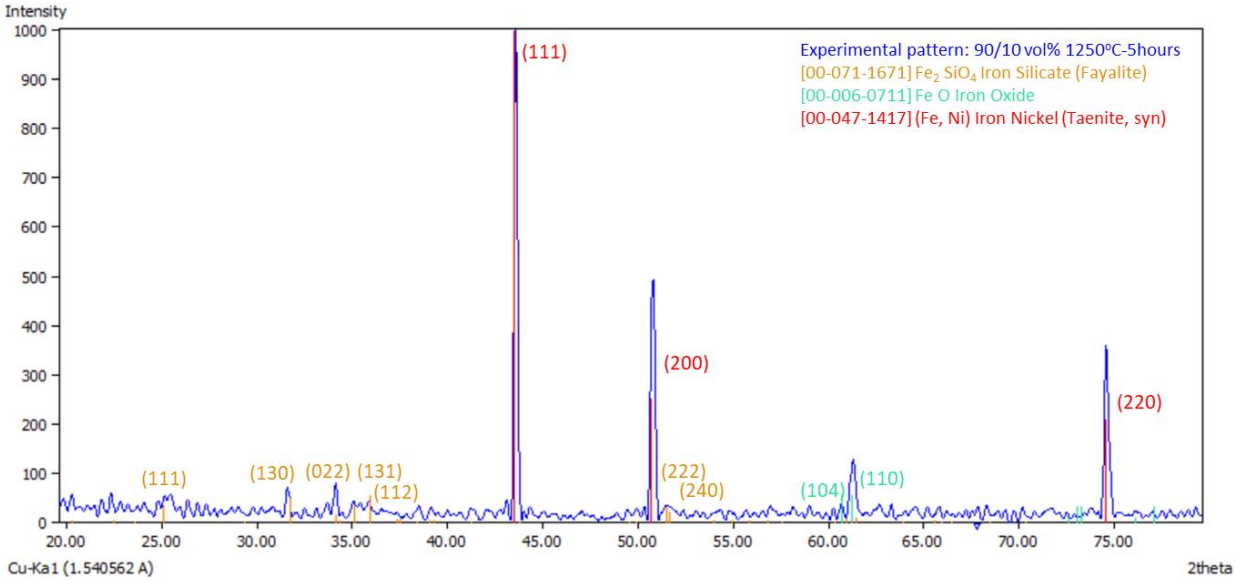

Density

A key aspect of this study was to be able to reduce the density of the Invar composite by varying the ratio of silica. One parameter affecting the density of the composites was the use of binder. The use of either CMC in H_2O or PVDF in NMP resulted in different levels of sintering as can be seen from Figure 9. Both pressed pellets of pure Invar had a density of 5.87g/cm^3 prior to sintering, but after sintering, the percent of theoretical densities were 84% and 89% for the CMC/H_2O and PVDF/NMP, respectively. It is believed that the higher density achieved by the PVDF in NMP is due to better compatibility of solvent with the powders. Suspending the powders in a CMC and H_2O solution and then slowly drying, could have led to oxidation on the surface of the powder. This oxidation would then hinder the ability of the powders to sinter. Oxidation on the surface of sintered samples was already observed if the sample was not properly dried after polishing, therefore it is suspected that the CMC/H_2O binder solution could have caused some oxidation in the bulk of the sample.

Figure 9: Experimental Density vs. Silica Composition for Samples using Different Binders

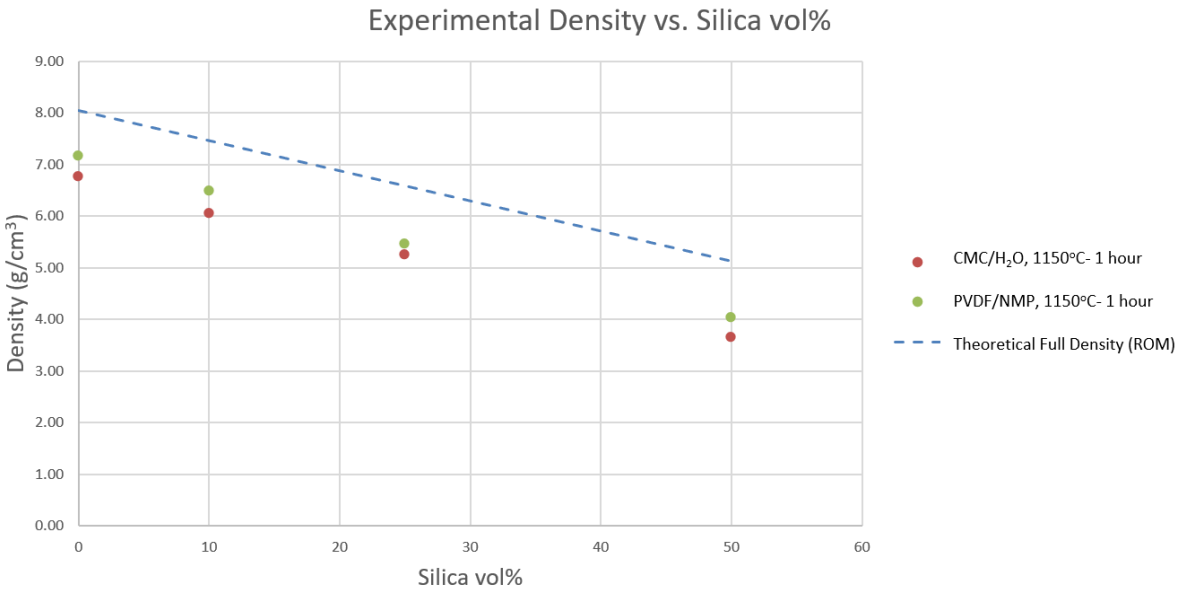

The use of binder added a variable which affected the sintering ability of the composites. The samples with binder were held at 500°C for an hour before ramping up to the sintering temperature. However, this was done under inert atmosphere conditions so higher temperatures may have been needed to completely remove the binder from the samples. The use of a binder presented two concerns: the complete removal of the binder and possible reactions between the binder solution and the ball milled powder. It was these concerns that led to moving towards the use of no binder in the samples. This proved difficult as cracks often formed in many of the 60/40 and 50/50 samples during pressing. However, the use of no binder would give a better understanding of the parameters necessary to reach the highest theoretical density possible for the composites.

It should be noted that some variability is due to the different densities of the pressed pellets prior to sintering. The densities of the unsintered samples were calculated by measuring the dimensions and mass of the pellets. There was more variability in the 60/40 and 50/50 densities

due to the formation of cracks. The average pressed densities for each composition as well their standard deviation are shown in Table 3 below.

Table 3: Average Pressed Density per Sample Composition

Invar/Silica vol%	Pure	90/10	75/25	60/40	50/50
Density (g/cm^3)	6.11	5.67	4.69	3.17	3.08
Standard Deviation	0.16	0.16	0.13	0.65	0.39

After sintering, the densities of the samples were measured using Archimedes method and compared to the theoretical full density calculated using Rule of Mixtures (ROM). Below in Table 4 are the density results for different sintering parameters and in parenthesis is the percent of theoretical density.

Table 4: Density Results for Sintering Parameters of Each Sample Set

Sample Set		1	2	3	4	5	6	7	8
vol% Silica	Theoretical Full Density (ROM)	CMC/H_2O 1200°C-1hr	PVDF/NMP 1150°C-1hr	CMC/H_2O 1150°C-1hr	No Binder, 1250°C-1hr	No Binder, 1275°C-1hr	No Binder, 1250°C-5hrs	No Binder, 1100°C-2hr	No Binder, 1150°C-3hrs
0	8.05	6.75 (84%)	7.15 (89%)	6.77 (84%)	7.23 (90%)	7.23 (90%)	7.44 (92%)	6.35 (79%)	6.77 (84%)
10	7.47	5.98 (80%)	6.48 (87%)	6.04 (81%)	6.96* (93%)*	6.81* (91%)*	--*	6.16 (82%)	6.60 (88%)
25	6.59	4.81 (73%)	5.46 (83%)	5.26 (80%)	6.11 (93%)	5.88 (89%)	6.06 (92%)	5.40 (82%)	5.59 (85%)
40	5.71	--	--	--	--	5.07 (89%)	5.37 (94%)	--	5.24 (92%)
50	5.13	--	4.03 (79%)	3.65 (71%)	4.73 (92%)	4.55 (89%)	4.79 (93%)	4.42 (86%)	4.44 (87%)

*- indicates the sample had phase separation on the surface

The sample sets with the best results can be seen in Figure 10 where the blue dashed line is the theoretical full density. These sample sets were later characterized further.

Figure 10: Experimental Density vs. Silica Composition

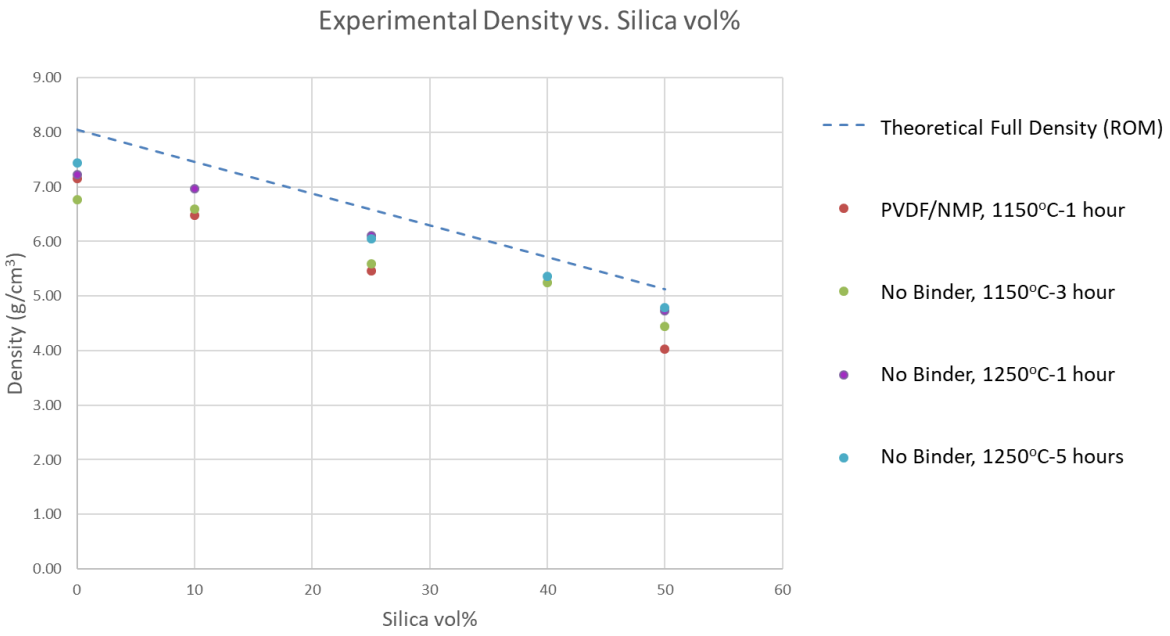

Approximately 90-94% of theoretical density was achieved for each of the samples sintered at 1250°C regardless of the composition. For the PVDF/NMP 1150°C-1hr, sintering was affected by the amount of silica in the samples where 89% of theoretical density was attained for pure Invar whereas only 79% was achieved for the 50/50 sample. This is most likely due to the higher melting temperature of silica (T_m=1713°C) compared to that of Invar (T_m=1430°C). The temperature was high enough to sinter the Invar but not the silica. By increasing the sintering time for the 1150°C, the densities of the higher concentration silica samples could be increased.

The 1250°C-5hrs samples showed the best overall density results, however there was phase separation on the surface of all the 90/10 samples sintered at 1250°C. The formation of this new phase raises concerns about sintering at this high of a temperature for this composition. The 1150°C-3hr samples showed good density results across the whole range of compositions and the reduced sintering temperature avoided phase separation in the 90/10 sample.

Microstructure Characterization

The distribution of silica powder within the Invar can have a significant impact on the properties of the sintered composite. Any agglomeration of the silica could lead to problems with the level of sintering of the composite as well as later issues with the printing resolution when using additive manufacturing. Scanning Electron Microscopy (SEM) was used to characterize the microstructure of the samples and how it varied with the addition of silica. Below in Figure 11 are the images of the 100/0, 75/25, and 50/50 PVDF/NMP samples heated to 1150^{o}C for 1 hour.

Figure 11: SEM Images for PVDF/NMP Binder, 1150^{o}C-1hr

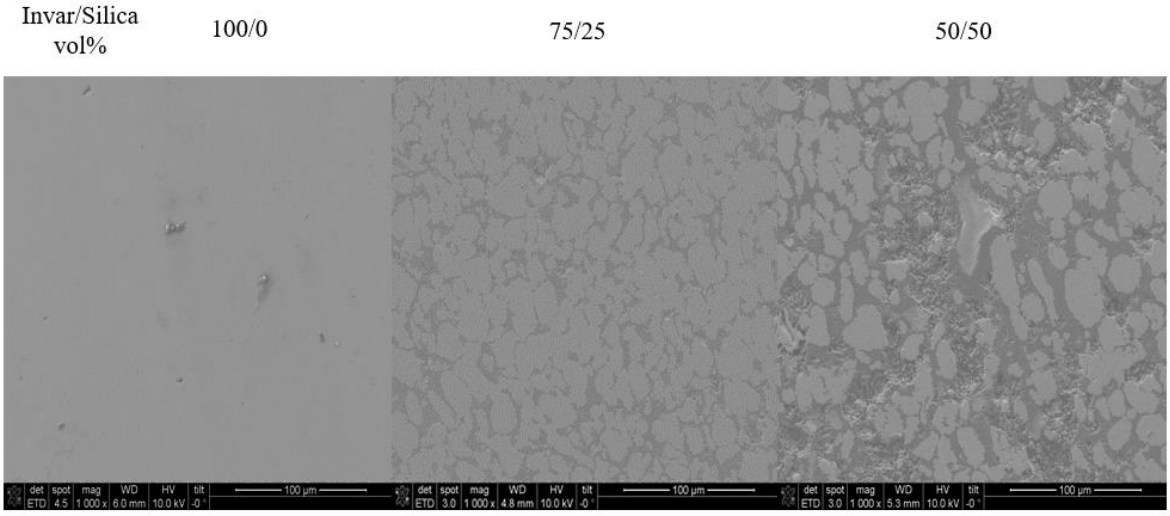

The SEM of the pure Invar sample appears well-sintered with minimal voids (89% theoretical density). The images of the 75/25 and 50/50 samples (center and right) help give information of the microstructure of the composite. The Invar appears to sinter while the silica is accumulated at the grain boundaries. The silica-rich regions are not fully sintered, and voids can be seen in certain areas. The higher melting point of silica is likely the reason these regions were

not able to completely sinter. Due to the slow ramping rate for the tube furnace (~3 ^{o}C/min), the silica had significant time to diffuse out to the grain boundaries. Fortunately, the silica is dispersed throughout the material with no formation of large agglomerates. Ideally, the composite would have silica more homogenously dispersed throughout the Invar.

The 1150^{o}C-3hrs and 1250^{o}C-5hrs samples both attained a high level of sintering. SEM images of the samples can allow for a comparison of the two resulting microstructures. A comparison of the 50/50 microstructures of the 1250^{o}C-5hrs and 1150^{o}C-3hrs can be seen below.

Figure 12: 50/50 vol% Invar/Silica Samples 1150^{o}C-3hrs (left), 1250^{o}C-5hrs (right)

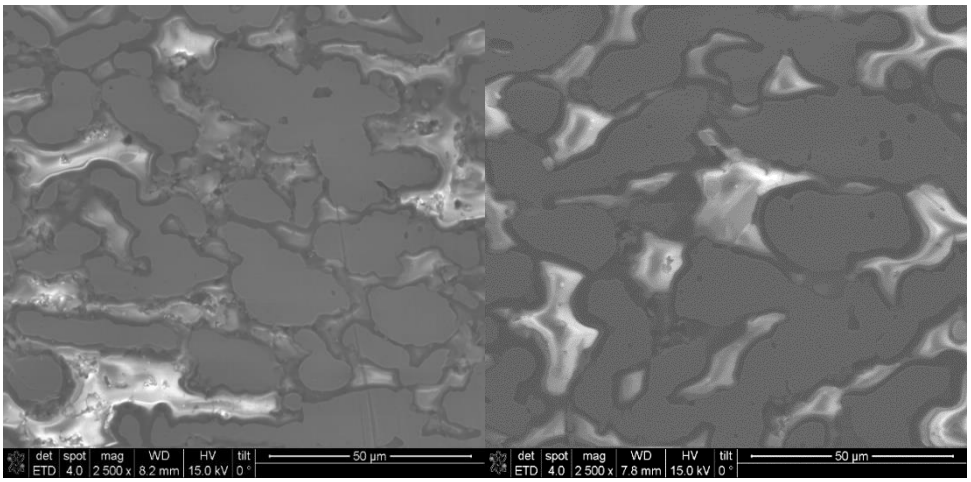

Both samples show similar grain size and shape with the voids mainly occurring in the silica-rich regions. The silica and Invar remain two separate, unreacted phases which was later confirmed using other characterization techniques. Both the Invar and silica sintered in the 50/50 samples, however the silica-rich regions appear denser in the 1250^{o}C-5hrs sample. This could also explain the difference in densities observed where 1250^{o}C for 5hrs had a higher density (93%) than the 1150^{o}C 3hrs (87%). The sintering parameters of 1250^{o}C-5hrs allowed the silica to sinter

more completely. The SEM images of the composites also show that even in the 50/50 samples, the Invar matrix remains a connected network. This proves to be important especially when considering certain properties such as electrical resistivity or CTE.

Energy-Dispersive X-ray Spectroscopy

Energy-Dispersive X-ray Spectroscopy (EDX) was performed on the surface of one of the 90/10 samples showing phase separation. Other 90/10 samples sintered at lower temperatures showed no such phase separation, so it was important to determine what unanticipated phase had formed at the surface of the sample. A region of the 90/10 vol% Invar/Silica 1250^{o}C-5hr sample was scanned and the compositions are shown in Figure 15 below. There is no Ni present in the separated phase. This reinforces the XRD results suggesting the formation of an iron silicate phase. Therefore, the combination of XRD and EDX results identified the phase separating out on the surface of the sample to be iron silicate.

Figure 13: EDX of Compositions of 2 Regions on the Surface of 90/10 vol% Invar/Silica Sintered at 1250^{o}C for 5 hours (a) an image of the region scanned (b) Composition of Point 1 Showing No Presence of Ni (c) Composition of Point 2 Showing Ni in the Bulk of the Sample

a)

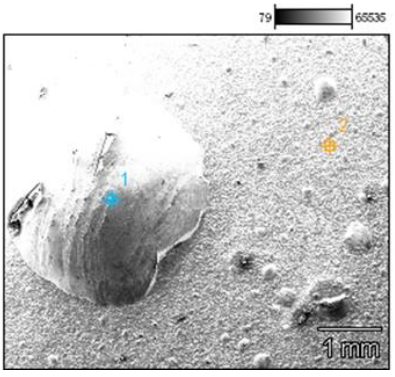

Image Name:	Mnr det shift test(3)
Image Resolution:	512 by 442
Image Pixel Size:	12.17 µm
Acc. Voltage:	12.0 kV
Magnification:	50

b)

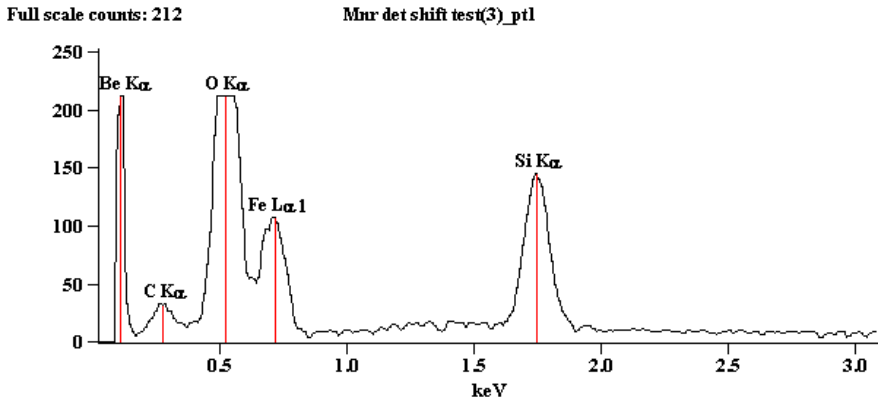

c)

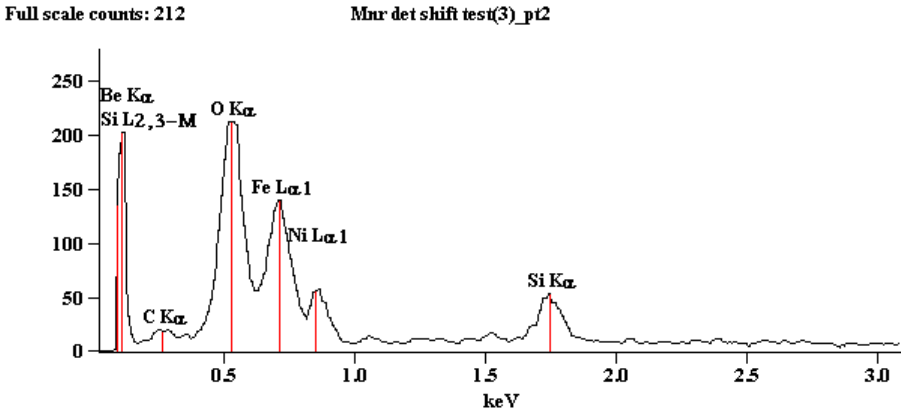

EDX of a polished cross-section of a 50/50 1150^{o}C-1hr sample gave more information on the dispersion of silica in the samples. Results from the 50/50 sample in Figure 16 confirm the darker regions at the grain boundaries seen in SEM, are silica-rich. The lighter grains seen in SEM are Invar grains containing little silica. These results give a better overall picture of the compatibility of the Invar-silica composite. While the Invar and silica don't appear to have reacted to form any new phases, the silica is not homogenously dispersed.

Figure 14: EDX for 50/50 Composition Sintered at 1150°C for 1 hour

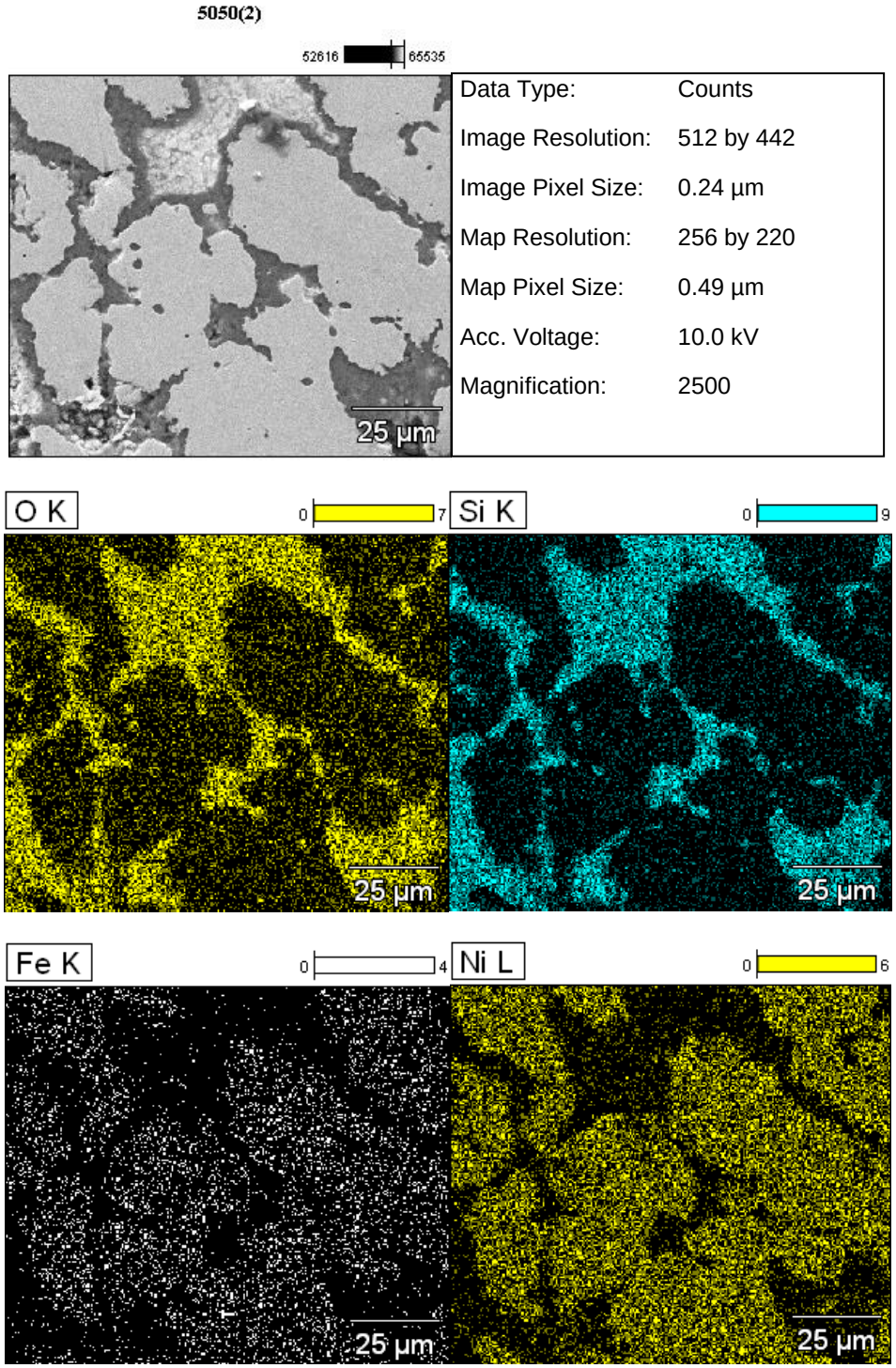

Since an iron silicate phase was found on the surface of the 90/10 sample, it could possibly be forming in the bulk of the other samples at this temperature. Therefore, a cross section of the

50/50 sample at 1250ºC-5hrs was scanned in order to determine if new phases were forming in the bulk. As can be seen in Figure 17 below, the Invar and silica phases remain separate and unreacted. Therefore, the Fe silicate phase appears to only have formed on the 90/10 samples which could indicating the phase forms more easily at 10 vol% silica composition.

Figure 15: EDX for 50/50 Composition Sintered at 1250ºC for 5 hours

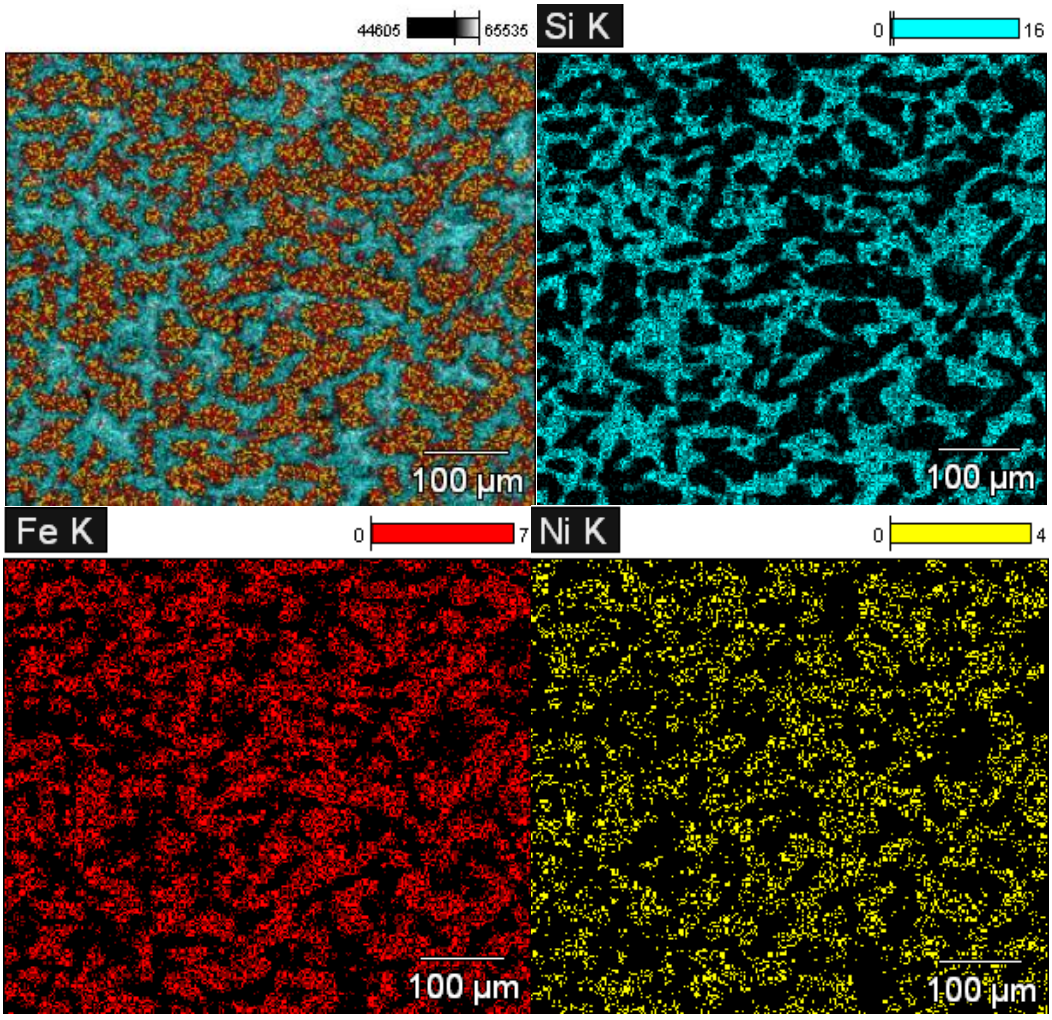

Electrical Resistivity

The electrical resistivity of the samples was measured with a multimeter across approximately 2mm on the surface of the polished samples. The multimeter only gave a resistivity accurate to $\pm 0.1\Omega$ so the values should be viewed comparatively across the different silica compositions. For reference, pure Invar is known to have a resistivity on the order of $10^{-8}\Omega\bullet m$, while silica is not electrically conductive with a resistivity greater than $10^{18}\Omega\bullet m$. The electrical resistivity of the pure Invar samples were magnitudes higher than the reference value. This is most likely due to the contact of the probes as well as the porosity in the samples. However, all the samples were conductive with very low resistivities even for the 50/50 samples. This indicates the Invar metal matrix remained continuous even at high silica compositions. Table 5 below lists the resistivity values for both the 1150°C-3hrs and 1250°C-5hrs samples. The 1250°C samples demonstrate a higher resistivity possibly due to the more complete sintering of silica which could begin to impede the connectivity of the Invar metal matrix. Overall, the electrical resistivity of the composites did not increase significantly, only by a factor of 1.7 when comparing 50/50 to that of pure Invar.

Table 5: Electrical Resistivity based on Silica Composition

	Electrical Resistivity ($\Omega\bullet m$)	
Invar/Silica vol%	1150°C-3hrs	1250°C-5hrs
100/0	6×10^{-4}	8×10^{-4}
90/10	8×10^{-4}	--
75/25	8×10^{-4}	8×10^{-4}
60/40	8×10^{-4}	8×10^{-4}
50/50	1×10^{-3}	1×10^{-3}

Coefficient of Thermal Expansion

The coefficient of thermal expansion (CTE) was measured using a Netzsch Dilatometer 402PC. The sample sets sintered at 1150^{o}C for 3 hours and 1250^{o}C for 5 hours were measured from 30^{o}C to 300^{o}C at a ramp rate of 5^{o}C/min. The test was run with argon flowing at 5 mL/min after purging for an hour, however the dilatometer was not airtight. The samples showed some oxidation after the test which could have resulted in a higher CTE. The sample thickness would also lead to some variability since oxidation on a thinner sample would have a larger effect on the measured displacement or CTE.

Below in Figure 18 are the displacement curves versus temperature for each composition sintered at 1150^{o}C for 3 hours. The average CTE was then calculated across three temperature ranges: 30-100 ^{o}C, 100-150 ^{o}C, and 150-250 ^{o}C as seen in Figure 19 and Table 6. Generally, an increase in silica composition led to an increase in the CTE.

Figure 16: Displacement Curves for 1150^{o}C-3hrs Samples at Different Invar/Silica vol% Ratios

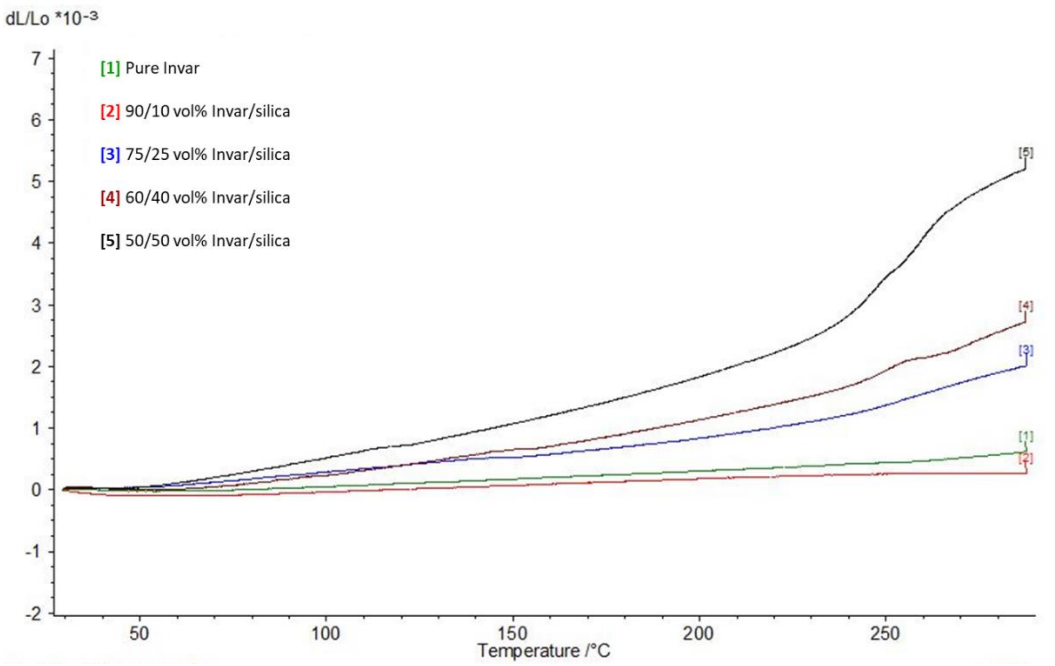

Figure 17: Average CTE for Across Different Temperature Ranges for Samples Sintered at 1150ºC for 3 hours

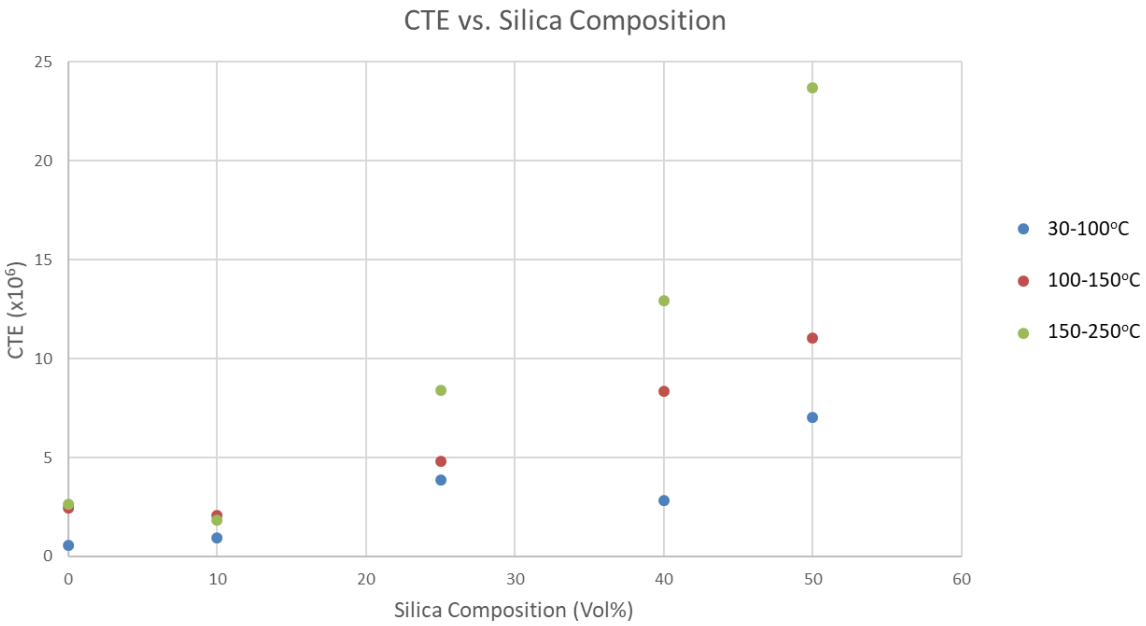

Table 6: Average CTE Values Across Different Temperature Ranges for Samples Sintered at 1150ºC for 3 hours

Silica Composition (vol%)	CTE ($x10^{-6}$) for 30-100ºC	CTE ($x10^{-6}$) for 100-150ºC	CTE ($x10^{-6}$) for 150-250ºC
0	0.57	2.44	2.65
10	0.93	2.10	1.84
25	3.89	4.82	8.39
40	2.82	8.36	12.94
50	7.05	11.04	23.69

The increase in coefficient of thermal expansion with higher silica composition was most likely due to the phase transformation of silica during sintering. Amorphous silica has a CTE of 0.55 x 10^{-6} from 20-100ºC however the CTE of cristobalite and tridymite are approximately 11 x

10^{-6} and 25 x 10^{-6} respectively. [17-18] Based on the XRD results, the amorphous silica is believed to devitrify during sintering. The CTE's of crystalline silica are higher than that of Invar (~1.2 x 10^{-6}) therefore the overall CTE of the composite would be expected to increase.

For comparison, the samples sintered at 1250°C for 5 hours were then tested. Figure 20 shows the displacement curves versus temperature for each composition. The average CTE was also calculated across the three temperature ranges and are shown in Figure 21 and Table 7. Once again, there was a general increase in CTE with an increase in silica composition. However, the CTE values in this sample set were significantly lower compared to those sintered at 1150°C for 3 hours. This is believed to be due to the greater level of sintering and lower porosity achieved.

Figure 18: Displacement Curves for 1250°C-5hrs Samples at Different Invar/Silica vol% Ratios

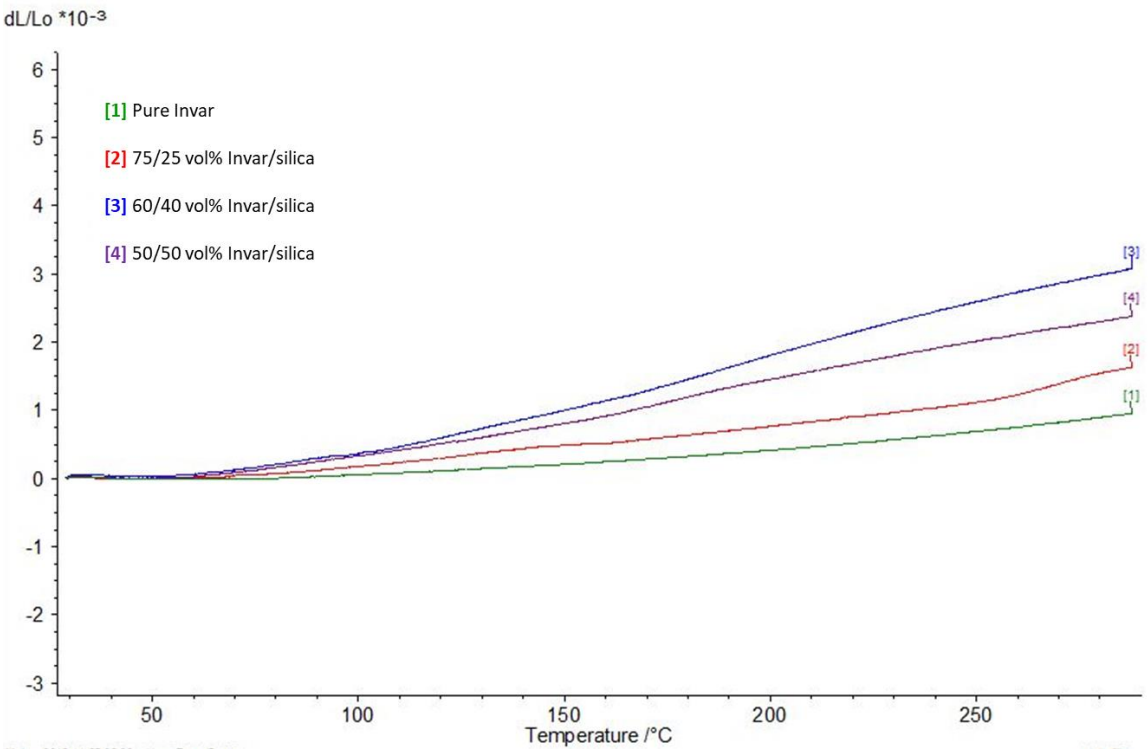

Figure 19: Average CTE for Across Different Temperature Ranges for Samples Sintered at 1250ºC for 5 hours

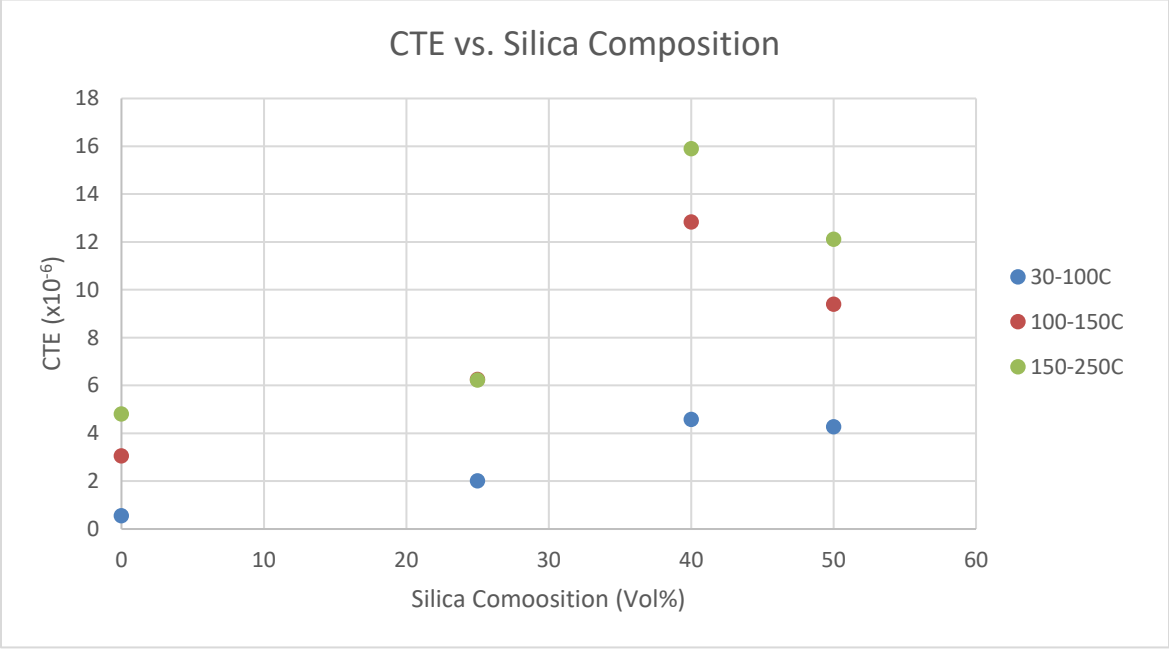

Table 7: Average CTE Values Across Different Temperature Ranges for Samples Sintered at 1250ºC for 5 hours

Silica Composition (Vol%)	CTE ($x10^{-6}$) for 30-100ºC	CTE ($x10^{-6}$) for 100-150ºC	CTE ($x10^{-6}$) for 150-250ºC
0	0.56	3.07	4.81
25	2.02	6.26	6.23
40	4.59	12.85	15.91
50	4.28	9.41	12.13

Conclusion

Metal matrix composites comprised of Invar and silica were produced with the goal of obtaining a density and CTE lower than that of pure Invar. Different ratios of Invar and silica were ball milled, pressed into pellets and sintered. The compositions ranged from 0-50vol% silica and the Rule of Mixtures was used to calculate the theoretical density of the composites. The sintering temperature and time were varied in order to find the sintering parameters yielding the best results for the composites. When sintered at 1250^{o}C for 5 hours, densities as high as 7.44 g/cm^{3} (92% of theoretical) and 4.79 g/cm^{3} (93% of theoretical) were achieved for pure Invar and the 50/50 composite respectively. SEM images show Invar grains surrounded by silica-rich regions at the grain boundaries, later confirmed by EDX. Higher temperatures were required to sinter these silica-rich regions in the composites. Phase separation was observed on the surface of 90/10 vol% samples sintered at temperatures above 1200^{o}C, requiring this composition to be sintered at a lower temperature. XRD was used to identify the desired γ-Fe, Ni phase was obtained and that there was no oxide or iron silicate forming in the bulk of the composite. Results from an XRD scan of a 50/50 vol% sample found the amorphous silica to be devitrifying. The 50/50 vol% composite only increased in electrical resistivity by a factor of 1.7 compared to pure Invar, remaining conductive with a continuous Invar matrix. The CTE of the composites increased with the addition of silica due to the formation of crystalline forms of silica which have a larger CTE than that of Invar.

Outlook for Additive Manufacturing

One possible challenge with the formation of these composites is the different temperatures needed to sinter the components. Ideally the silica would be well-dispersed in the Invar phase and

the Invar would be able to sinter around the silica. Attaining Invar and silica powders that are of similar size is one factor that would help achieve better homogeneity. This would then allow for lower temperatures than what would be needed for the pure silica to sinter. However, in the case of the composites in this study, the silica had accumulated at the grain boundaries. Therefore, higher temperatures are needed to sinter these silica-rich regions and achieve closer to theoretical density.

The devitrification of amorphous silica to cristobalite and tridymite led to an increase in the CTE of the composite. Ideally this phase change would be avoided during the sintering of the composite. It is possible that an additive manufacturing method could be a means to do this by limiting the phase change kinetically. Ultimately, the processing conditions for the additive manufactured composite will be different than the cold-pressing and sintering approach investigated. Although, this study gives a good indication of the compatibility of the two materials as well as its expected properties.

References

[1] Shapiro, A. A., et al. “Additive Manufacturing for Aerospace Flight Applications.” Journal of Spacecraft and Rockets, vol. 53, no. 5, 2016, pp. 952–959., doi:10.2514/1.a33544.

[2] Yap, C. Y., et al. “Review of Selective Laser Melting: Materials and Applications.” Applied Physics Reviews, vol. 2, no. 4, 2015, p. 041101., doi:10.1063/1.4935926.

[3] Frazier, William E. “Metal Additive Manufacturing: A Review.” Journal of Materials Engineering and Performance, vol. 23, no. 6, 2014, pp. 1917–1928., doi:10.1007/s11665-014-0958-z.

[4] Guillaume, Ch. Ed. “Invar and Its Applications.” Nature, vol. 71, no. 1832, 1904, pp. 134–139., doi:10.1038/071134a0.

[5] Sokolowski, Witold M., et al. “Dimensional Stability of High-Purity Invar 36.” Quality and Reliability for Optical Systems, 1993, doi:10.1117/12.164978.

[6] Harrison, Neil J., et al. “Thermal Expansion Coefficients in Invar Processed by Selective Laser Melting.” Journal of Materials Science, vol. 52, no. 17, 2017, pp. 10517–10525., doi:10.1007/s10853-017-1169-4.

[7] Hidalgo, J., et al. “Mechanical and Functional Properties of Invar Alloy Forμ-MIM.” Powder Metallurgy, vol. 57, no. 2, 2013, pp. 127–136., doi:10.1179/1743290113y.0000000081.

[8] Qiu, Chunlei, et al. “Selective Laser Melting of Invar 36: Microstructure and Properties.” Acta Materialia, vol. 103, 2016, pp. 382–395., doi:10.1016/j.actamat.2015.10.020.

[9] Zhan, Xiaohong, et al. “Quantitative Research on Microstructure and Thermal Physical Mechanism in Laser Melting Deposition for Invar Alloy.” Journal of Manufacturing Processes, vol. 31, 2018, pp. 221–231., doi:10.1016/j.jmapro.2017.11.018.

[10] Qi, J., and J. W. Halloran. “Negative Thermal Expansion Artificial Material from Iron-Nickel Alloys by Oxide Co-Extrusion with Reductive Sintering.” Journal of Materials Science, vol. 39, no. 13, 2004, pp. 4113–4118., doi:10.1023/b:jmsc.0000033391.65327.9d.

[11] Chawla, N., and Y.-L. Shen. “Mechanical Behavior of Particle Reinforced Metal Matrix Composites.” Advanced Engineering Materials, vol. 3, no. 6, 2001, pp. 357–370., doi:10.1002/1527-2648(200106)3:63.3.co;2-9.

[12] Wu, D., et al. “Preparation of Cu/Invar Composites by Powder Metallurgy.” Powder Metallurgy, vol. 58, no. 2, 2014, pp. 100–105., doi:10.1179/1743290114y.0000000098.

[13] Gaspera, Enrico Della, et al. “Copper-Based Conductive Composites with Tailored Thermal Expansion.” ACS Applied Materials & Interfaces, vol. 5, no. 21, 2013, pp. 10966–10974., doi:10.1021/am403227c.

[14] Ibrahim, I. A., et al. “Particulate Reinforced Metal Matrix Composites - a Review.” Journal of Materials Science, vol. 26, no. 5, 1991, pp. 1137–1156., doi:10.1007/bf00544448.

[15] Trujillo, J. E., et al. “Metal-Matrix Nanocomposites with Tailored Coefficients of Thermal Expansion for Improved Thermomechanical Reliability.” Journal of Electronic Materials, vol. 41, no. 6, 2011, pp. 1020–1023., doi:10.1007/s11664-011-1856-x.

[16] Kivi, Nicholas, et al. “Devitrification Rates of Fused Silica in the Presence of Trace Impurities.” University of Tennessee Knoxville, 2016.

[17] Austin J. B., et al. “The Coefficient of Linear Thermal Expansion of Tridymite.” Journal of the American Chemical Society (1954) 76 (23), 6019-6020

[18] Aumento F., “Stability, lattice parameters, and thermal expansion of β-cristobalite.” American Mineralogist 1966; 51 (7): 1167–1176.

[19] Koike, C., et al. “Infrared Spectra Of Silica Polymorphs And The Conditions Of Their Formation.” The Astrophysical Journal, vol. 778, no. 1, 2013, p. 60., doi:10.1088/0004-637x/778/1/60.

[20] Rancourt, D. G., and M.-Z. Dang. “Relation between Anomalous Magnetovolume Behavior and Magnetic Frustration in Invar Alloys.” Physical Review B, vol. 54, no. 17, 1996, pp. 12225–12231., doi:10.1103/physrevb.54.12225.